Journal of Alloys and Compounds 509 (2011) 9271–9277

Contents lists available at ScienceDirect

Journal of Alloys and Compounds

journal homepage: www.elsevier.com/locate/jallcom

Factors controlling pure-phase magnetic $BiFeO_3$ powders synthesized by solution combustion synthesis

Jun Yang [a,*], Xiaoci Li [a], Junyi Zhou [a], Yu Tang [a], Yuanming Zhang [a], Yongwang Li [b]

[a] Department of Chemistry, Jinan University, Guangzhou 510632, People's Republic of China
[b] State Key Laboratory of Coal Conversion, Institute of Coal Chemistry, Chinese Academy of Sciences, Taiyuan 030001, People's Republic of China

ARTICLE INFO

Article history:
Received 9 May 2011
Received in revised form 5 July 2011
Accepted 10 July 2011
Available online 19 July 2011

Keywords:
Combustion synthesis
X-ray diffraction
$BiFeO_3$
Nanopowders
Fuel-to-oxidant ratio

ABSTRACT

Bismuth ferric oxide nanopowders were prepared through combustion method. Pure phase and well-crystallized $BiFeO_3$ can be obtained by controlling the combustion process, fuel type and fuel-to-oxidant ratio. The evolutions of phase constitution and structural characteristics of the as-resulted nanopowders were investigated by X-ray diffraction, scanning electron microscope, and simultaneous thermogravimetric analysis. The results revealed that both the type and amount of fuel have to be carefully considered because they play an important role in total reaction characteristics. Among all tested fuels, L-α-alanine and glycine are the suitable fuels for $BiFeO_3$ synthesis. For α-alanine, the optimal fuel-to-oxidant ratio is 0.22, which results in a suitable flame temperature for $BiFeO_3$ formation. Still, too little fuel would result in only amorphous phase powders due to the low flame temperature and too much fuel would lead to transformation of the $BiFeO_3$ phase to impurities because of the high flame temperature involved. The resulting $BiFeO_3$ nanopowders exhibited strong H_2O_2-activiting ability and weak magnetism. When $BiFeO_3$ nanopowders were used as a heterogeneous Fenton-like catalyst to degrade rhodamine B (RhB), the apparent rate constant for RhB degradation in the presence of H_2O_2 at pH 5.0 was evaluated to be 0.048 min^{-1}.

1. Introduction

In recent years, multiferroics, showing the coexistence of magnetic and ferroelectric orders in a certain range of temperature, have attracted a great deal of attention due to the fascinating fundamental physics and potential applications in information storage, the emerging field of spintronics, and sensors [1]. Among all multiferroic materials studied so far, $BiFeO_3$ (BFO) is one of the well-known multiferroic compounds having simultaneous ferroelectric and G-type antiferromagnetic orders over a broad range above room temperature (Curie temperature > 800 °C, Neel temperature = 370 °C) [2–5]. In addition to the potential magnetoelectric applications, BFO might find applications as photocatalytic materials due to its small bandgap [1,6,7].

Previous studies have demonstrated that synthesis of $BiFeO_3$ nanoparticles via a traditional solid-state method produces poor reproducibility and causes formation of Bi_2O_3/$Bi_2Fe_4O_9$ impurity phase [8]. In the solid state route, Bi_2O_3 and Fe_2O_3 are reacted at a temperature in the range of 800–830 °C and unreacted Bi_2O_3, impurity phases $Bi_2Fe_4O_9$ and $Bi_{25}FeO_{40}$ are removed by washing in HNO_3. The crystallization temperature of BFO for this method is too high to avoid bismuth loss.

The ceramic $BiFeO_3$ phase pure compound is very difficult to achieve. Secondary phases like Bi_2O_3, $Bi_2Fe_4O_9$ and $Bi_{25}FeO_{39}$ are reported to systematically appear due to the kinetics of phase formation. In recent years, the synthesis of $BiFeO_3$ nanomaterials has been achieved by various techniques, including hydrothermal synthesis [9–12], polymer-assisted hydrothermal synthesis [13], microwave–hydrothermal synthesis [14], mineralizer-assisted hydrothermal synthesis [15], microwave-induced solid-state decomposition [16], sol–gel process [17–19], Pechini [20] and modified Pechini method [21], molten-salt method [22,23], sonochemical and microemulsion techniques [24], co-precipitation [25–28], EDTA complexing sol–gel process [29], polymeric precursor method [30,31], ferrioxalate precursor method [32], polymer-directed solvothermal route [33], polyacrylamide gel route [34] and tartaric acid-assisted gel strategy [35]. However, each of these methods has its own advantages and limitations. To our knowledge, complex process control, high reaction temperature or long synthesis time may be required for these approaches. From a practical viewpoint, the development of simpler, energy efficient and environmentally benign procedures to obtain $BiFeO_3$ nanopowder with a regular morphology and a homogeneous chemical composition is still an active area of research.

* Corresponding author. Tel.: +86 20 85220223; fax: +86 20 85220223.
E-mail addresses: tyangj@jnu.edu.cn, tyangj@126.com (J. Yang).

0925-8388/$ – see front matter © 2011 Elsevier B.V. All rights reserved.
doi:10.1016/j.jallcom.2011.07.023

Among the various wet chemical processes, the combustion route is found to be a versatile, simple and rapid process, which allows effective synthesis of a variety of nanosize materials [36]. This method relies on the exploitation of the combustion reaction enthalpy, which is taking place when rapidly heating a mixture containing the desired metal nitrates and various organic fuels. The highly exothermic nature of the reaction ensures the self-propagating character of the combustion process. The temperature reached within the reactant system is high enough to promote the formation of the desired compound without any additional annealing. Pure crystalline $MgAl_2O_4$ was synthesized from the combustion reaction by using fuel mixtures containing urea and monoethanolamine or urea and β-alanine, no additional calcination being necessary [37]. Lanthanum-based perovskite oxide powders, $LaFeO_3$ and $LaMnO_3$, were produced by aqueous combustion synthesis using two different fuels [38]. A pure phase fully densified $La_{0.8}S_{r0.2}CrO_3$ (LSC) perovskite membrane was synthesized by aqueous combustion method using the metal nitrates (oxidizer)–glycine (fuel) system [39]. Fine particle perovskite oxides such as $LnCrO_3$ (where Ln = La, Pr, Nd, Sm, Dy, Gd, and Y), $La_{1-x}Sr_xMnO_3$, $LaCoO_3$, and $LaNiO_3$ were prepared by the combustion of corresponding metal nitrate–tetraformal trisazine (TFTA) mixtures at 350 °C/500 °C in a few minutes under ambient conditions [40]. Orthorhombic structure perovskite $LaFeO_3$ nanocrystalline with size 27 nm were prepared by glycine combustion method [41]. Mixed-conducting oxide $SrFeCo_{0.5}O_y$ powders were synthesized by auto-combustion of citrate–nitrate gel [42]. Strontium-doped lanthanum manganite ($Li_{1-x}Sr_xMnO_3$) powders were synthesized by a solution combustion method using a unique combination of oxidant and fuel, nitrate–acetate stoichiometrically [43]. However, so far, to the best of our knowledge, there are few reports on the preparation of pure $BiFeO_3$ using combustion method [44,45].

It is well known that physicochemical properties of the oxide powders synthesized by combustion process are mainly depending on the nature and the amount of fuel that used [46,47]. However, a systematic approach towards fuel and fuel-to-oxidant ratio selection for $BiFeO_3$ synthesis is still lacking. Some authors [48] failed to obtain single phase $BiFeO_3$ nanopowders directly from the combustion reaction. As a consequence, the previously combustion-synthesized powders were annealed at different temperatures in order to ensure the formation of $BiFeO_3$.

The combustion method is based on the mixing of reactants that oxidize easily, such as metal nitrates, and an organic fuel, acting as a reducing agent. An external heat supply is needed to initiate the ignition of the mixture leading to a self-sustainment of an exothermic redox reaction. Therefore, both the types and amounts of fuel have to be carefully considered because they play an important role in total reaction characteristics. The aim of this paper is to systematically investigate the effect of fuel-type and fuel-to-oxidant ratio on morphology, composition, size and shape of the product in the synthesis of crystalline $BiFeO_3$ perovskite nanopowders, and obtain pure-phase $BiFeO_3$ nanopowders right from low-temperature combustion synthesis.

2. Experimental

2.1. Materials and synthesis

The starting raw materials were analytical grade purity and were used as received without further purification. Bismuth nitrate [$Bi(NO_3)_3{\cdot}5H_2O$] and iron nitrate [$Fe(NO_3)_3{\cdot}9H_2O$] were used as oxidizing agents, whereas citric acid ($C_6H_8O_7{\cdot}6H_2O$), urea (CON_2H_4), stearic acid ($C_{18}H_{36}O_2$), glycine ($C_2H_5NO_2$), ethylene glycol ($C_2H_6O_2$), ethanolamine (C_2H_7NO), sucrose($C_{12}H_{22}O_{11}$), L-α-alanine ($C_3H_7NO_2$), L-aspartic acid ($C_4H_7NO_4$), L-valine ($C_5H_{11}NO_2$) and L-leucine ($C_6H_{13}NO_2$) were used as fuels.

Equi-molar mixtures of $Bi(NO_3)_3{\cdot}5H_2O$ and $Fe(NO_3)_3{\cdot}9H_2O$ were dissolved in diluted HNO_3 to form aqueous solution. The appropriate amount of fuel was then added to the above solution, respectively, and the mixture was stirred until complete dissolution occurred. The fuel-to-oxidant ratio was derived from the total oxidizing and reducing valences of the oxidizer and fuel using the concepts of propellant chemistry [49]. In a theoretical stoichiometric composition, oxidizing valence provided by the oxidizer is equal to reducing valence from the fuel. Every step mentioned above was accompanied by constant magnetic stirring to make the solution transparent and homogeneous. The resultant solution was transferred into a ceramic crucible and kept at 80 °C for 8 h in a vacuum oven till it became a dark viscous resin, and then placed in a muffle furnace at 300 °C. The viscous resin bubbled up and auto-ignited with the rapid evolution of a large volume of gases. The whole process was over after several minutes, but the time between the actual ignition and the end of the reaction was less than 20 s. After the combustion is over in furnace, it is further heated for 5–10 min to allow complete combustion of material. Finally, as-synthesized products were taken out of furnace and grinding was done to achieve finer powder. The crystal structure of the synthesized powder was characterized.

2.2. Characterization

The viscous resin was subjected to thermogravimetric analyzer (TGA 4000, PerkinElmer, USA) to determine the temperature of possible reaction. The samples were heated at a rate 10 °C/min up to 600 °C under air flow. The morphologies were observed with a scanning electron microscope (SEM, JEOL JSM-6330F, Japan) operated at an accelerating voltage of 20 kV. The crystalline phases of the samples were identified by X-ray diffraction (XRD, Siemens D-5000) with a graphite monochromator and Cu Kα1 (λ = 0.15406 nm) radiation operating at 36 kV, 20 mA. The type of scanning was 2θ–θ mode with a speed of 8° min^{-1} in the range of 10°–80°. The crystallite size was determined based on the XRD patterns (*h k l* planes: 1 0 1, 0 1 2 and 1 1 0) using the Sherrer's equation: $D = 0.89\lambda/(\beta\cos\theta)$, where D is the crystallite size in nm, λ is the radiation wavelength (Cu Kα1, 0.15406 nm), β is the full width at half of the maximum in radians and θ is the Bragg-angle. The magnetic properties (M–H curve) were measured at 300 K on an ADE 4HF vibrating sample magnetometer.

2.3. Photocatalytic degradation experiment

The photocatalytic activity was evaluated by the degradation of rhodamine B (RhB) in aqueous solution under visible-light irradiation using a 175 W metal halide lamp with a cut-off filter (λ > 400 nm). The reaction temperature was kept at room temperature by cooling water to prevent any thermal catalytic effect. In each experiment, aqueous suspension of 100 mL RhB with the concentration of 10 mg L^{-1} and 0.1 g $BiFeO_3$ powder (1 g L^{-1}) was placed in a reactor under vigorous stirring. The suspension was magnetically stirred in dark for 30 min to achieve the adsorption/desorption equilibrium between the solution and catalyst. The RhB concentration after equilibration was measured and taken as the initial concentration (c_0). Then, the degradation reaction was initiated by adding 0.1 mL H_2O_2 (30%) under magnetic stirring conditions. Solution samples were taken at a given time intervals during the reaction and centrifuged, the RhB concentration in the supernatant was determined by using a UV–visible spectrophotometer (TU1801, PGENERAL)

3. Results and discussion

3.1. Effect of fuel type on the combustion synthesis of $BiFeO_3$

The elemental stoichiometry of each combustion reaction was calculated using the concepts of propellant chemistry. According to the method proposed by Jain et al. [49], the initial composition of the solution containing bismuth nitrate, iron nitrate and fuel was derived from the total reducing and oxidizing valences of the fuel and oxidizer. Carbon, hydrogen, bismuth and iron were considered as reducing species with corresponding valences of +4, +1, +3 and +3, respectively. Oxygen was considered an oxidizing element with valence of −2, and nitrogen was considered to be 0. In the case of glycine–nitrate combustion, the total calculated valences of metal nitrates by arithmetic summation of the oxidizing and reducing valences was −30. The calculated valence of glycine was +9.

The theoretical stoichiometric composition of the glycine–nitrate redox mixture demanded the presence of $1\times(-30)+n\times(+9)=0$, or $n = 3.33$ mol in the reaction. Assumed that in the case of glycine–nitrate combustion, primarily N_2, CO_2, and H_2O are evolved as the gaseous products, the stoichiometric redox reaction can be expressed as follows:

$$Bi(NO_3)_3{\cdot}5H_2O + Fe(NO_3)_3{\cdot}9H_2O + 3.33C_2H_5NO_2 = BiFeO_3 + 6.66CO_2 + 22.33H_2O + 4.66N_2 \quad (1)$$

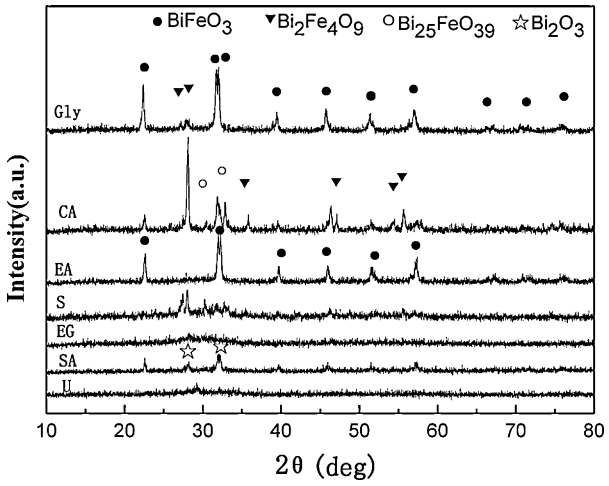

Fig. 1. X-ray diffraction patterns of the powders prepared from $Bi(NO_3)_3$, $Fe(NO_3)_3$ and various fuels by combustion synthesis.

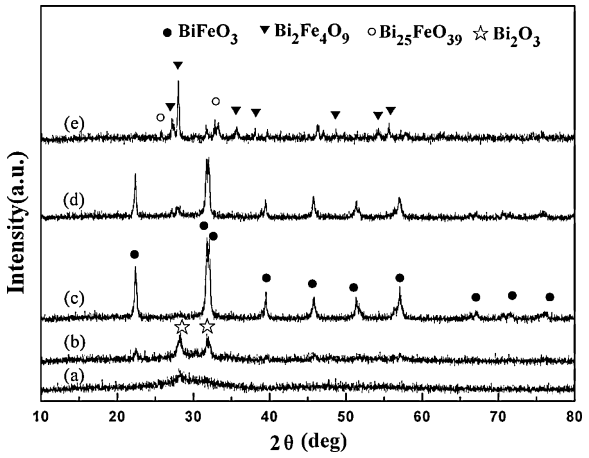

Fig. 2. X-ray diffraction patterns of as-synthesized powders using glycine with various fuel-to-oxidant molar ratios: (a) Gly/NO_3^- = 0.19 fuel-lean (−66%); (b) 0.28 fuel-lean (−50%); (c) 0.37 fuel-lean (−34%); (d) 0.56 stoichiometric; (e) 0.84 fuel-rich (+50%).

The number of moles of gases produced per mole of oxide ($BiFeO_3$) formation is about 33.65. The fuel-stoichiometric composition indicates Gly/NO_3^- = 0.56 (glycine-to-nitrate ion ratio), while fuel-lean composition range shows Gly/NO_3^- < 0.56 and fuel-rich composition range means Gly/NO_3^- > 0.56, respectively. In our work, this so-called stoichiometric composition is actually a fuel-lean composition, because the diluted HNO_3 (2 mL, 2 mol/L) was added to dissolve $Bi(NO_3)_3{\cdot}5H_2O$.

The theoretical stoichiometric fuel-to-oxidizer ratio ($Fuel/NO_3^-$) of different fuels, including urea, stearic acid, ethylene glycol, sucrose, ethanolamine and citric acid was calculated in the same manner as glycine–nitrate system.

Fig. 1 shows the XRD patterns of the powders prepared using various fuels in stoichiometric fuel-to-oxidant ratio at 300 °C. The synthesis using citric acid (CA) or sucrose (S) as fuel resulted in two kinds of impurities ($Bi_{25}FeO_{39}$ and $Bi_2Fe_4O_9$), whereas the powder obtained using urea (U) or ethylene glycol (EG) had amorphous structure. In the case of the oxides prepared using stearic acid (SA) as fuel, a mixture of $BiFeO_3$ and Bi_2O_3 was obtained. When glycine (Gly) and ethanolamine (EA) were employed as fuels, one can easily observe that majority of the peaks belong to rhombohedral perovskite $BiFeO_3$ phase (according with JCPDS 86-1518, 74-2493 or 73-0548) along with other impurities phases such as $Bi_{25}FeO_{39}$ and $Bi_2Fe_4O_9$ in BFO powder. It is obvious that among all the tested fuels, ethanolamine and glycine are the most suitable fuel that allows the formation of $BiFeO_3$ directly from the combustion reaction. In contrast to this, Farhadi et al. [45] very recently tested various organic fuels including urea, citric acid, glycine and sucrose to synthesize $BiFeO_3$ by combustion method and found that sucrose ($C_{12}H_{22}O_{11}$) is the best fuel and resulted in the formation of pure and nano-size $BiFeO_3$ powder.

3.2. Amino acid approach for the combustion synthesis of $BiFeO_3$

The combustion reaction can be explosive, yielding a high flame which quickly propagates through the reactant mixture. Therefore, safety becomes more and more important when many grams of powder have to be prepared by auto-combustion synthesis, as observed by other authors [50,51]. In this work, the combustion reaction employed EA as fuel is the most explosive and a lot of powders are displaced from the combustion crucible, which leads to product lost.

Considering the experimental result presented above and the safety conditions, it can be inferred that glycine is a more appropriate fuel for synthesizing $BiFeO_3$. However, the as-synthesized powders obtained at theoretical stoichiometric fuel-to-oxidant ratio are not pure $BiFeO_3$. In order to verify the effect of fuel type and fuel-to-oxidant ratio on the characteristics of as synthesized powders, we systematically tested various amino acid, for example, glycine, L-α-alanine, L-aspartic acid, L-valine and L-leucine.

The XRD patterns of the as-prepared powders with various glycine-to-oxidant molar ratios (Gly/NO_3^-) are shown in Fig. 2. It can be seen that Gly/NO_3^- plays an important role in the formation of pure $BiFeO_3$ powder. When Gly/NO_3^- = 0.19 (fuel-lean reaction, −66%), only a mixture of amorphous phase and Bi_2O_3 phase was obtained, which indicates the incomplete combustion of precursors. With the increase of Gly/NO_3^-, the phase transformation of amorphous phase to $BiFeO_3$ and Bi_2O_3 happened, and two phases $BiFeO_3$ and Bi_2O_3 were obtained in the 0.28 Gly/NO_3^- ratio (−50%). At Gly/NO_3^- = 0.37 (fuel-lean reaction, −34%), nearly all of the Bi_2O_3 and amorphous phases were transformed to $BiFeO_3$. Only the peaks corresponding to perovskite-type $BiFeO_3$ (JCPDS Card No. 86-1518) were recognized, whereas no peaks attributable to Bi_2O_3 and/or Fe_2O_3 and unreacted precursor materials were detectable. The mean crystallite size of $BiFeO_3$ calculated by the Sherrer's equation was about 28 nm. By increasing Gly/NO_3^- to above 0.56 (theoretical stoichiometric), $Bi_{25}FeO_{40}$ and $Bi_2Fe_4O_9$ phase was observed.

Fig. 3 presents the XRD patterns of the powders prepared with different α-alanine-to-oxidant molar ratios (α-Ala/NO_3^-). It is revealed that the $BiFeO_3$ nanopowder is highly crystallized and exhibits a single-phase perovskite structure in the 0.22 α-Ala/NO_3^- ratio (fuel-lean reaction, −33%). Non-perovskite phases such as $Bi_2Fe_4O_9$ and Bi_2O_3/Fe_2O_3 are not detected in XRD spectra. The crystallite size of the powders is about 32 nm. When α-Ala/NO_3^- = 0.17 (−50%), only amorphous phase powders were obtained. By increasing α-Ala/NO_3^- to above 0.33 (theoretical stoichiometric), gradual transformation of the $BiFeO_3$ phase to the $Bi_{25}FeO_{39}$ and $Bi_2Fe_4O_9$ phase occurred. Fig. 4 shows the X-ray diffraction patterns of as-synthesized powders with various L-Asp-to-oxidant, L-Val-to-oxidant and L-Leu-to-oxidant ratios. It is obviously seen that pure $BiFeO_3$ powders can not be obtained using these three kinds of amino acid under both fuel-lean and fuel-rich conditions.

Amino acids contain a carboxylic acid group at one end and an amino group at the other end; they become zwitter ions on dissolving in water with both a positive and negative charges. Such types of zwiterionic character of amino acid molecule can effectively complex metal ions of varying ionic sizes, which helps in preventing their selective precipitation to maintain compositional

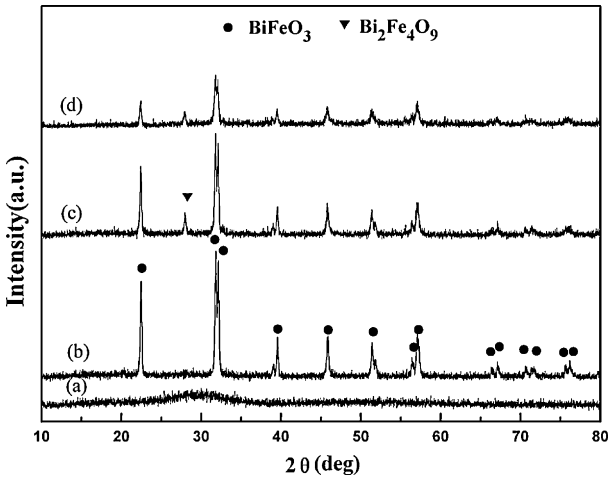

Fig. 3. X-ray diffraction patterns of as-synthesized powders using α-alanine with various fuel-to-oxidant ratios: (a) α-Ala/NO_3^- = 0.17 fuel-lean (−50%); (b) 0.22 fuel-lean (−33%); (c) 0.33 stoichiometric; and (d) 0.50 fuel-rich (+50%).

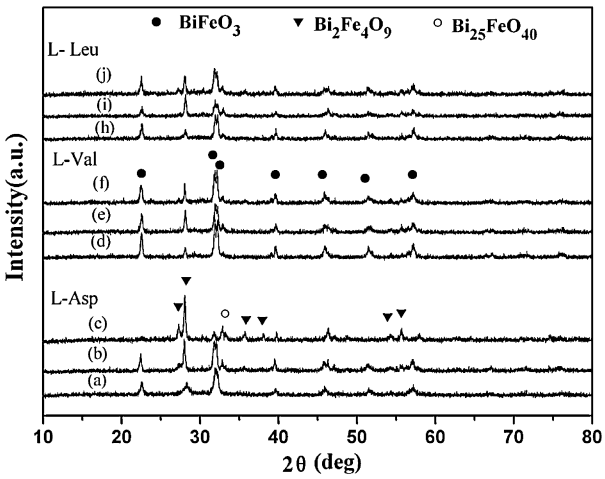

Fig. 4. X-ray diffraction patterns of as-synthesized powders with various fuel-to-oxidant molar ratios: (a) L-Asp/NO_3^- = 0.22 fuel-lean (−33%); (b) 0.33 stoichiometric; (c) 0.5 fuel-rich (+50%); (d) L-Val/NO_3^- = 0.12 fuel-lean (−33%); (e) 0.19 stoichiometric; (f) 0.28 fuel-rich (+50%); (h) L-Leu/NO_3^- = 0.10 fuel-lean (−33%); (i) 0.15 stoichiometric; (j) 0.30 fuel-rich (+50%).

homogeneity among the constituents. On the other hand, amino acid can also serve as a fuel during a combustion reaction, being oxidized by nitrate ions [52,53]. Glycine is known to act as a strong complexing agent for a number of metal ions [54]. Glycine forms stable gel with mixed nitrate solutions of bismuth and iron and the combustion of the gel produces phase pure nano-crystalline powder. α-Alanine is a common amino acid used as a reducing fuel to achieve synthesize of ferrites at low temperature. It belongs to the same amino acid series as glycine, but unlike glycine it has an

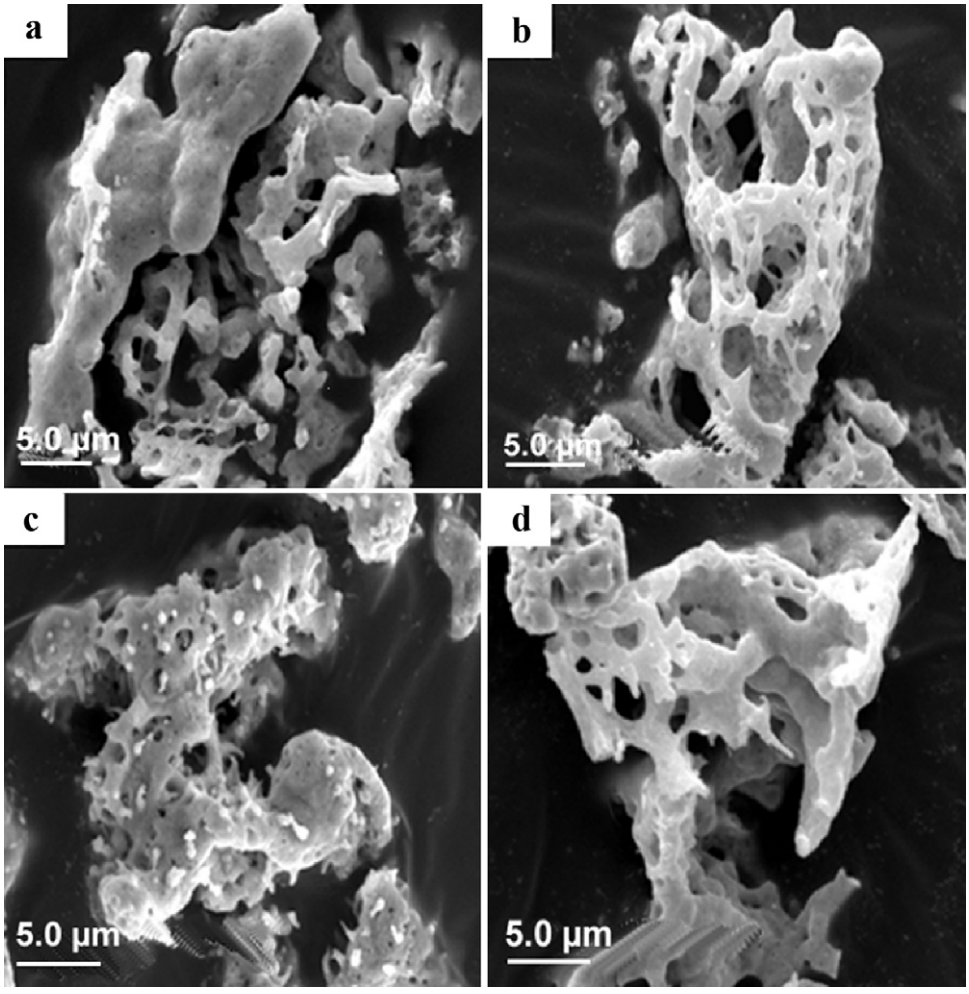

Fig. 5. SEM photographs of as-synthesized powders with various fuels (a) Gly/NO_3^- = 0.37 (fuel-lean reaction); (b) Gly/NO_3^- = 0.56 (stoichiometric reaction); (c) α-Ala/NO_3^- = 0.22 (fuel-lean reaction); (d) α-Ala/NO_3^- = 0.33 (stoichiometric reaction).

extra branched methyl group that might cause evolution of a large quantity of gases during combustion resulting in fine particles [55]. Moreover, alanine undergoes chelation with both trivalent bismuth and iron ions facilitating the chelation process that precedes the combustion reaction. With extra branched methyl group increase, it may cause the combustion temperature to reduce, because of the massive gases, carrying off the quantity of heat.

It is well-known that that $BiFeO_3$ is unstable in the vicinity of 800–850 °C and slowly decomposes [25,56]. The synthesis area of single-phase $BiFeO_3$ in the phase diagram of Bi_2O_3–Fe_2O_3 is very narrow from the view point of thermodynamics, in which two kinds of impurities ($Bi_2Fe_4O_9$ and $Bi_{25}FeO_{39}$) are the usual substitutions for $BiFeO_3$ [25]. Carvalho and Taveres [57] found that $BiFeO_3$ is a metastable phase at 600 °C, and thermal treatments longer than 2 h result in decomposition of $BiFeO_3$ accompanied by the formation of impurities, $Bi_2Fe_4O_9$ and $Bi_{25}FeO_{39}$ phases according to the reaction

$$49BiFeO_3 \rightarrow 12Bi_2Fe_4O_9 + Bi_{25}FeO_{39}.$$

which indicates that $BiFeO_3$ is not thermodynamically stable at this temperature.

The auto-ignition phenomena exist for a limited range of fuel-to-oxidant ratio, above and below the stoichiometric ratio calculated by the concept of propellant chemistry [49]. As we know, combustion synthesis is a complicated process. The flame temperature depends strongly on the competition between the effect of the amount of released heat and evolved gases [58]. Nair et al. [59] found that the flame temperature increases with fuel-to-oxidant ratio up to a certain limit close to the stoichiometric ratio and then its value decreases. This is because of the incomplete combustion of fuel-rich precursor caused by the presence of insufficient oxidizer for the burning the fuel. Ianos et al. [47] found that due to urea partial consumption during the hydrolysis side-reaction, 50% of urea excess is required in order to favour full combustion reaction and reduce the LOI (loss on ignition), and the use of urea excess above 150% of the stoichiometric ratio increased the surface area of the final powder. Ghosh et al. [60] synthesized calcium hydroxyapatite by combustion with urea and glycine as fuels. They found that the maximum combustion temperature was observed when stoichiometric fuel was used. Fuel-lean system produced short duration, less intense flame, whereas fuel-rich system produced longer duration lower temperature flame. The effect of different fuels and fuel-to-oxidant ratios on crystallographic phases and powder characteristics was extensively investigated for many oxides. The optimal oxidant-to-fuel ratio depends upon the desired composition [61]. In this study, the optimal fuel-to-oxidant ratio (F/NO_3^-) of α-alanine and glycine for pure-phase $BiFeO_3$ synthesis is 0.22 (fuel-lean reaction, −33%) and 0.37 (fuel-lean reaction, −34%), respectively, which results in a suitable flame temperature that favors the formation of $BiFeO_3$ phase. Still, too little fuel would result in only amorphous phase powders due to the low flame temperature and too much fuel would lead to transformation of the $BiFeO_3$ phase to impurities ($Bi_2Fe_4O_9$ and $Bi_{25}FeO_{39}$ phases) because of the high flame temperature involved.

The SEM photographs of as-prepared $BiFeO_3$ nanopowders are shown in Fig. 5. They revealed foamy agglomerated particles with a wide distribution and presence of large voids in their structure. The formation of these features is attributed to the large volume of gas evolved during combustion. No significant differences came out of the fuel-to-oxidant ratios from the morphologies examined with the SEM.

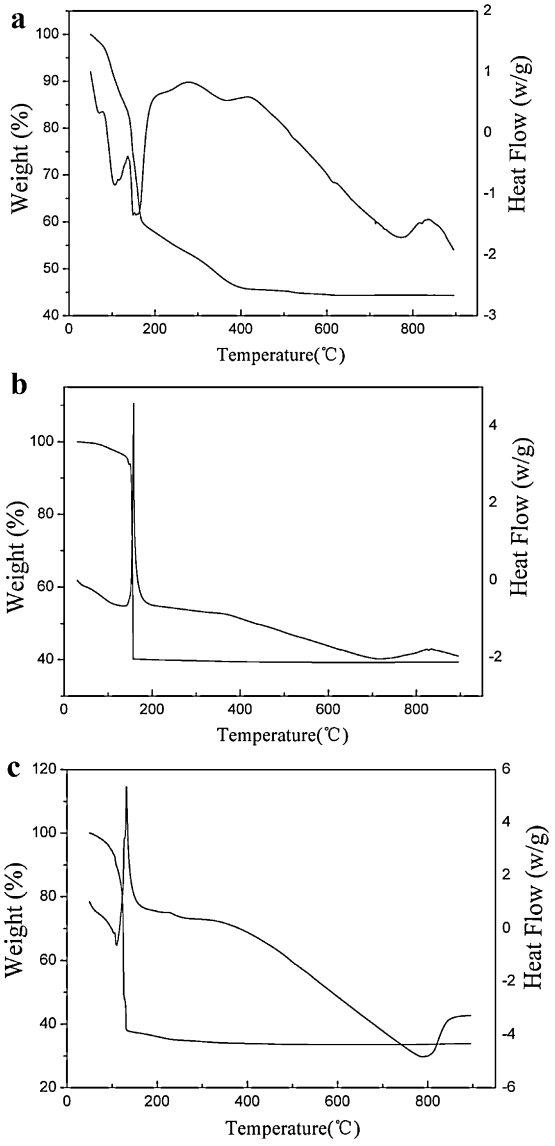

Fig. 6. TG-DSC curves of the precursor mixtures consisting of bismuth nitrate, iron nitrate and various fuels under stoichiometric fuel-to-oxidant condition: (a) without fuel, (b) α-alanine, and (c) L-leucine.

3.3. Thermal analysis of the precursors

Thermal analysis of the precursor mixture consisting of bismuth nitrate, iron nitrate and different fuels allowed the determination of some of the processes and phenomena which are taking place during the heating of the raw material mixture. As can be seen from Fig. 6, for the resin without fuel, three endothermic decomposition steps were evidenced in the temperature range of 50–600 °C (Fig. 6a). The first decomposition step (50–140 °C) is weight loss of 18%, which is a partial dehydration, namely the evolving water molecules as a consequence of the differently bounding of these molecules. The second step between 140 and 163 °C is weight loss of 22%, which is due to volatilization of nitrates in the gel residual. The final is weight loss of 15% extending up to 550 °C due to nitrate decomposition process. In the case of $Bi(NO_3)_3{\cdot}5H_2O$–$Fe(NO_3)_3{\cdot}9H_2O$–L-α-alanine precursors, the thermal decompositions are described by the existence of two main degradation stages (Fig. 6b). The first one, starts from ∼50 up to ∼150 °C being characterized by a mass loss of 7%. The second one (150–170 °C) accompanied by an exothermic peak is drastic weight

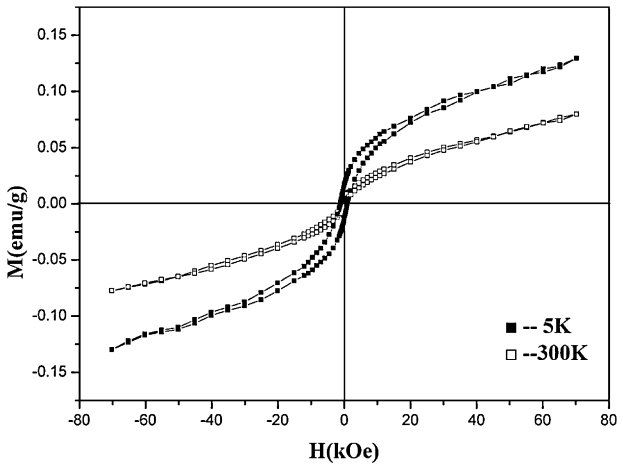

Fig. 7. M–H hysteresis loops for the $BiFeO_3$ nanopowders measured at 5 K and 300 K.

loss of 53%, which indicates that auto-propagating combustion reaction occurs during the decomposition of the resin. Almost no mass loss could be observed after the combustion reaction. In the case of $Bi(NO_3)_3{\cdot}5H_2O$–$Fe(NO_3)_3{\cdot}9H_2O$–L-leucine, the combustion reaction appears at about 130 °C accompanied by a drastic weight loss of 63%, and no further weight loss up to 230 °C.

3.4. Magnetism

The M–H loops of the $BiFeO_3$ prepared through combustion reaction by using α-alanine at 0.22 fuel-to-oxidant ratio were shown in Fig. 7. Weak magnetism can be observed in the powders. Bulk $BiFeO_3$ is a G-type antiferromagnet at room temperature and does not exhibit magnetism in the M–H curve [25].

3.5. Catalytic activity of $BiFeO_3$ nanopowders

In this work, rhodamine B, a common azo-dye in the textile industry, is chosen as a typical organic pollutant. The RhB degradation catalyzed by $BiFeO_3$ nanopowders was carried out in the presence of H_2O_2 at pH 5.0. It is well-known that RhB degradation approximately followed a pseudo first order reaction in kinetics, which can be replaced as: $\ln(C_0/C) = kt + \text{constant}$, where C_0 is the initial concentration of RhB solution, k is a rate constant and t is reaction time.

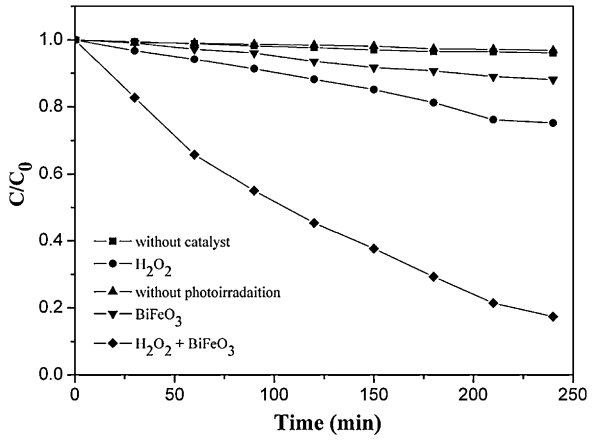

Fig. 8. Changes of RhB concentration as a function of irradiation time under visible light irradiation. Reaction conditions: initial RhB concentration 10 mg L^{-1}, initial H_2O_2 concentration 10 mmol L^{-1}, catalyst load 1.0 g L^{-1}, and initial solution pH 5.0.

As shown in Fig. 8, RhB is hardly degraded in the absence of either $BiFeO_3$ nanopowders or H_2O_2, but the simultaneous presence of $BiFeO_3$ nanopowders and H_2O_2 remove 85.1% of RhB within 240 min. The apparent rate constant of RhB degradation was evaluated to be 0.048 min^{-1}.

4. Conclusions

Single-phase and well-crystallized bismuth ferric oxide ($BiFeO_3$) nanopowders were successfully synthesized via a combustion method at low temperature, using both α-alanine and glycine as fuel. Both the type and amount of fuel strongly affect the phase composition and crystallinity of the as-synthesized product. An optimization of these parameters could improve the quality of the final products. Thermal analysis investigations revealed that the fuel-lean precursor (−33%) containing metal nitrates and α-alanine triggers a vigorous combustion reaction at 160 °C. In this case, pure-phase and well-crystallized $BiFeO_3$ nanopowders with a crystallite size of 32 nm were obtained directly from combustion reaction and an additional annealing process was no longer required.

Acknowledgement

The authors gratefully acknowledge financial support from the Team Project of Guangdong Province Natural Science Foundation (Grant No. 05200555).

References

[1] F. Gao, X.Y. Chen, K.B. Yin, S. Dong, Z.F. Ren, F. Yuan, T. Yu, Z.G. Zou, J.M. Liu, Adv. Mater. 19 (2007) 2889–2892.
[2] W. Eerenstein, N.D. Mathur, J.F. Scott, Nature 442 (2006) 759–765.
[3] H.W. Jang, D. Ortiz, S.H. Baek, C.M. Folkman, R.R. Das, P. Shafer, Y.B. Chen, C.T. Nelson, X.Q. Pan, R. Ramesh, C. Eom, Adv. Mater. 21 (7) (2009) 817–823.
[4] N. Hur, S. Park, P.A. Sharma, J.S. Ahn, S. Guha, S.W. Cheong, Nature 429 (2004) 392–395.
[5] J. Wang, J.B. Neaton, H. Zheng, V. Nagarajan, S.B. Ogale, B. Liu, D. Viehland, V. Vaithyanathan, D.G. Schlom, U.V. Waghmare, N.A. Spaldin, K.M. Rabe, M. Wuttig, R. Ramesh, Science 299 (2003) 1719–1722.
[6] Z.K. Liu, Y.J. Qi, C.J. Lu, J. Mater. Sci. Mater. Electron. 21 (4) (2010) 380–384.
[7] C.M. Cho, J.H. Noh, I.S. Cho, J.S. An, K.S. Hong, J.Y. Kim, J. Am. Ceram. Soc. 91 (11) (2008) 3753–3755.
[8] Y.P. Wang, L. Zhou, M.F. Zhang, X.Y. Chen, J.M. Liu, Z.G. Liu, Appl. Phys. Lett. 84 (2004) 1731–1733.
[9] C. Chen, J.R. Cheng, S.W. Yu, L.J. Che, Z.Y. Meng, J. Cryst. Growth 291 (2006) 135–139.
[10] S. Basu, M. Pal, D. Chakravorty, J. Magn. Magn. Mater. 320 (2008) 3361–3365.
[11] J.H. Luo, P.A. Maggard, Adv. Mater. 18 (2006) 514–517.
[12] S.H. Han, K.S. Kim, H.G. Kim, H.G. Lee, H.W. Kang, J.S. Kim, C. Il Cheon, Ceram. Int. 36 (2010) 1365–1372.
[13] Y.G. Wang, G. Xu, Z.H. Ren, X. Wei, W.J. Weng, P.Y. Du, G. Shen, G.R. Han, Ceram. Int. 34 (2008) 1569–1571.
[14] J. Prado-Gonjal, M.E. Villafuerte-Castrejón, L. Fuentes, E. Morán, Mater. Res. Bull. 44 (2009) 1734–1737.
[15] Y.G. Wang, G. Xu, Z.H. Ren, X. Wei, W.J. Weng, P.Y. Du, G. Shen, G.R. Han, J. Am. Ceram. Soc. 90 (2007) 2615–2617.
[16] S. Farhadi, N. Rashidi, J. Alloys Compd. 503 (2010) 439–444.
[17] M. Kumar, K.I. Yadav, G.D. Varma, Mater. Lett. 62 (2008) 1159–1161.
[18] J.H. Xu, H. Ke, D.C. Jia, W. Wang, Y. Zhou, J. Alloys Compd. 472 (2009) 473–477.
[19] T.J. Park, G.C. Papaefthymiou, A.J. Viescas, A.R. Moodenbaugh, S.S. Wong, Nano Lett. 7 (2007) 766–772.
[20] E.A.V. Ferri, I.A. Santos, E. Radovanovic, R. Bonzanini, E.M. Girotto, J. Braz. Chem. Soc. 19 (2008) 1153–1157.
[21] S.M. Selbach, T. Tybell, M.A. Einarsrud, T. Grande, Chem. Mater. 19 (2007) 6478–6484.
[22] J. Chen, X.R. Xing, A. Watson, W. Wang, R.B. Yu, J.X. Deng, L. Yan, C. Sun, X.B. Chen, Chem. Mater. 19 (2007) 3598–3600.
[23] X.B. He, L. Gao, Ceram. Int. 35 (2009) 975–978.
[24] N. Das, R. Majumdar, A. Sen, H.S. Maiti, Mater. Lett. 61 (2007) 2100–2104.
[25] H. Ke, W. Wang, Y.B. Wang, J.H. Xu, D.C. Jia, Z. Lu, Y. Zhou, J. Alloys Compd. 509 (2011) 2192–2197.
[26] H.Y. Bo, G.Q. Tan, H.Y. Miao, A. Xia, Adv. Mater. Res. 105–106 (2010) 286–288.
[27] Z.K. Liu, Y.J. Qi, C.J. Lu, J. Mater. Sci. Mater. Electron. 21 (2010) 380–384.
[28] V.R. Palkar, D.C. Kundaliya, S.K. Malik, J. Appl. Phys. 93 (2003) 4337–4339.
[29] J. Wei, D.S. Xue, Mater. Res. Bull. 43 (2008) 3368–3373.
[30] M. Popa, D. Crespo, J.M. Calderon-Moreno, S. Preda, V. Fruth, J. Am. Ceram. Soc. 90 (2007) 2723–2727.

[31] S.M. Selbach, M.A. Einarsrud, T. Tybell, T. Grande, J. Am. Ceram. Soc. 90 (2007) 3430–3434.
[32] S. Ghosh, S. Dasgupta, A. Sen, H.S. Maiti, Mater. Res. Bull. 40 (2005) 2073–2079.
[33] L. Zhang, X.F. Cao, Y.L. Ma, X.T. Chen, Z.L. Xue, J. Solid State Chem. 183 (2010) 1761–1766.
[34] T. Xian, H. Yang, X. Shen, J.L. Jiang, Z.Q. Wei, W.J. Feng, J. Alloys Compd. 480 (2009) 889–892.
[35] X. Wang, Y.G. Zhang, Z.B. Wu, Mater. Lett. 64 (2010) 486–488.
[36] S.T. Aruna, A.S. Mukasyan, Curr. Opin. Solid State Mater. Sci. 12 (2008) 44–50.
[37] R. Ianos, I. Lazău, C. Păcurariu, P. Barvinschi, Eur. J. Inorg. Chem. 6 (2008) 931–938.
[38] T. Striker, J.A. Ruud, J. Am. Ceram. Soc. 93 (2010) 2622–2629.
[39] A.S. Mukasyan, C. Costello, K.P. Sherlock, D. Lafarga, A. Varma, Sep. Purif. Technol. 25 (2001) 117–126.
[40] S.S. Manoharan, K.C. Patil, J. Solid State Chem. 102 (1993) 267–276.
[41] S.M. Khetre, H.V. Jadhav, S.R. Bamane, RASĀYAN J. Chem. 3 (2010) 82–86.
[42] R.Q. Chu, Z.J. Xu, J. Electroceram. 21 (2008) 778–781.
[43] S. Saha, S.J. Ghanawat, R.D. Purohit, J. Mater. Sci. 41 (2006) 1939–1943.
[44] V. Fruth, L. Mitoseriu, D. Berger, A. Ianculescu, C. Matei, S. Preda, M. Zaharescu, Prog. Solid State Chem. 35 (2007) 193–202.
[45] S. Farhadi, M. Zaidi, J. Mol. Catal. A: Chem. 299 (2009) 18–25.
[46] R. Ianos, I. Lazău, C. Păcurariu, P. Barvinschi, Mater. Res. Bull. 43 (2008) 3408–3415.
[47] R. Ianos, I. Lazău, C. Păcurariu, J. Mater. Sci. 44 (2009) 1016–1023.
[48] C. Paraschiv, B. Jurca, A. Ianculescu, O. Carp, J. Therm. Anal. Calorim. 94 (2008) 411–416.
[49] S.R. Jain, K.C. Adiga, V.R.P. Vemeker, Combust. Flame 40 (1) (1981) 71–79.
[50] I.M. Tuukkanena, S.D. Brownb, E.L. Charsleyb, S.J. Goodallb, P.G. Layeb, J.J. Rooneyb, T.T. Griffithsc, H. Lemmetyinend, Thermochim. Acta 426 (2005) 115–121.
[51] F. Deganello, G. Marcì, G. Deganello, J. Eur. Ceram. Soc. 29 (2009) 439–450.
[52] R.D. Purohit, B.P. Sharma, K.T. Pillai, A.K. Tyagi, Mater. Res. Bull. 36 (2001) 2711–2721.
[53] J.C. Toniolo, M.D. Lima, A.S. Takimi, C.P. Bergmann, Mater. Res. Bull. 40 (2005) 561–571.
[54] L.A. Chick, L.R. Pederson, G.D. Maupin, J.L. Bates, L.E. Thomas, G.J. Exarhos, Mater. Lett. 10 (1990) 6–12.
[55] M.W. Raja, S. Mahanty, P. Ghosh, R.N. Basu, H.S. Maiti, Mater. Res. Bull. 42 (2007) 1499–1506.
[56] R. Palai, R.S. Katiyar, H. Schmid, P. Tissot, S.J. Clark, J. Robertson, S.A.T. Redfern, G. Catalan, J.F. Scott, Phys. Rev. B 77 (2008) 014110.
[57] T.T. Carvalho, P.B. Tavares, Mater. Lett. 62 (2008) 3984–3986.
[58] W.F. Chen, F.S. Li, J.Y. Yu, Mater. Lett. 60 (2006) 57–62.
[59] S.R. Nair, R.D. Purohit, A.K. Tyagi, P.K. Sinha, B.P. Sharma, Mater. Res. Bull. 43 (2008) 1573–1582.
[60] S.K. Ghosh, S.K. Roy, B. Kundu, S. Datta, D. Basu, Mater. Sci. Eng. B 176 (2011) 14–21.
[61] G. Singh, V.S. Tiwari, P. Tiwari, A.K. Srivastava, P.K. Gupta, J. Alloys Compd. 509 (2011) 4127–4131.